A SPHERICAL ENCODER FOR REAL-TIME MEASUREMENTS OF THREE-DOF WRIST ORIENTATIONS

Kok-Meng Lee and **Debao Zhou**
Georgia Institute of Technology
The George W. Woodruff School of Mechanical Engineering
Atlanta, GA 30332-0405
Tel: (404)894-7402; Fax: (404)894-9342; email: kokmeng.lee@me.gatech.edu

ABSTRACT: The need for simultaneous measurement of more-than-one degrees-of-freedom (DOF) motions of an object can be found in numerous applications such as robotic assembly, precision machining, optical tracking, wrist actuators, and active joysticks. Conventional single-axis encoders, though capable of providing high-resolution linear or angular measurements, require additional mechanical linkages that often introduce frictions, backlashes, and singularities. In this paper, a non-contact optical sensor for three-DOF orientation measurement is present. Unlike other contemporary designs, which often require a specific pattern to be drawn on a surface, this optical sensor presented here relies only on microscope features on natural surfaces to detect incremental motions. Here we offer a detailed description of the design and the development of a dual-sensor system capable of measuring three-DOF motions in real time. The analysis that is essential for optimizing the sensor design, has been validated experimentally.

1. INTRODUCTION

This paper presents an interesting optical sensor for measuring 3-DOF incremental motions in real time. This design concept was motivated by the development of a ball-joint-like spherical motor [Lee *et al.* 1996] as shown in Figure 1, which offers some attractive features by combining pitch, roll, and yaw in a single joint. Orientation measurement plays a significant role in the feedback control of a spherical motor as it could impose a limit on the system performance, particularly on the resolution and the sampling time.

A common method to measure the three-DOF rotor orientation is to use three single-axis encoders arranged in series or parallel as shown in Figure 1. The desire to eliminate the constraining mechanism has motivated Lee [1995] to develop alternative non-contact image-based methods to measure three-DOF orientation of a spherical body. Lee and his co-workers have led to the development of a vision-based wrist orientation sensor [Lee *et al.*, 1993; Garner *et al.*, 2001] as shown in Figure 2, and a flexible-integrated-vision-system [Lee and Blenis, 1994]. The three-DOF spherical encoder consists of a spherical grid pattern and an imaging sensor controlled by an on-board microprocessor. Since the absolute grid pattern can be printed on the surface of the spherical rotor, the optical sensor adds no inertia to the rotor dynamics. Furthermore, the two-dimensional (2D) bar-code-like grid pattern not only offers an effective method to recover the absolute orientation of the rotor but also a means to calibrate the rotor center. The tradeoff, however, is

that sophisticated image processing is needed. In addition, the lack of an appropriate vision system for machine applications has also posed a significant challenge to real-time implementation of such a vision-based wrist orientation sensor.
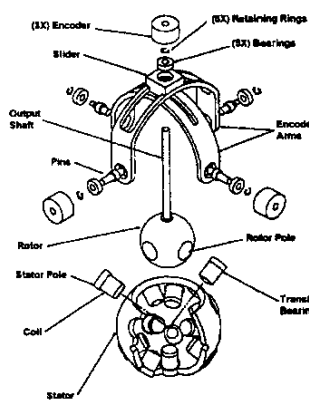

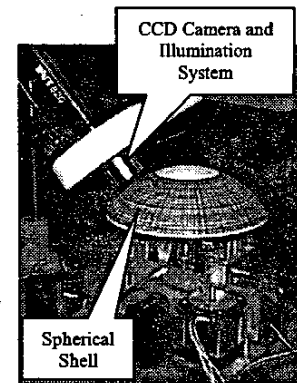Figure 1 Spherical motor with single-axis encoders

Figure 2 Universal wrist joint with a spherical encoder

Lee and Blenis [1994] have demonstrated that image processing frame rate of positional information can be drastically improved opto-mechatronically by optimally integrating optics, illumination, sensor, image signal processing hardware, and software for machine applications. Most recently, lucrative demands for high-performance pointing devices (such as a computer input mouse) for use with a personal computer have provided the incentives for the development of high-resolution optical sensors for measuring 2-DOF translational displacements [Bidlville, *et al.*, 1997]. The sensor for the pointing-device generates pulses proportional to the incremental sensor motion with respect to a static surface. The number of pulses is derived from the detection of microscopic changes between consecutive images; no engineered patterns (such as interferometer grating) are needed. While the optical sensor for a pointing-device is capable to detect changes with a high imaging frame-rate in the order of 1,500 frames per second (fps), the sensor is indifferent to the rotation about its optical axis. Lee and Zhou [2003] have developed a dual-sensor system for measuring the instantaneous center of rotation and the angular displacement of a moving plane, the success of which has provided us the incentives for further development of an optical encoder for measuring the three-DOF orientation of a spherical wrist actuator.

Specifically, this paper offers the following:

(1) We offer the design of a non-contact spherical encoder for measuring wrist orientation, which has no moving mechanism, and does not require precision grid patterns. Unlike a user-operated 2D pointing device that is indifferent to rotations about its own optical axis, the spherical encoder quantitatively measures the incremental three-DOF rotations for machine applications in real time.

(2) We present the sensor model that emulates the popular three-consecutive-single-axis-encoders. Both the forward and inverse kinematics of the dual-sensor system have been derived to emulate the popular three-consecutive-single-axis-encoder (as shown in Figure 1) that offers an intuitive way of measuring the wrist orientation but without the constraining mechanism. While the forward kinematics that computes the sensor output for a given motions is essential for design analyses, the inverse kinematics that recovers the wrist orientation from the instantaneous sensor output is essential for real-time measurements.

(3) A prototype spherical encoder has been developed and experimentally evaluated. The prototype spherical encoder has been experimentally evaluated using six different types of rotational motions on the wrist apparatus as shown in Figure 2.

(4) Sensor model has been experimentally validated. The sensor kinematics derived analytically has been experimentally validated. As will be shown, the model offers an effective means for study the effects of noises and to identify design parameters on the sensor performance.

2. OVERVIEW OF A 3-DOF SPHERICAL ENCODER

Figure 3(a) shows the optical path for the sensor, where the optics consist of a lens through which the sensor acquires surface images, an integral light pipe through which the LED provides the surface illumination, and a lens prism to focus the LED light at the optimal angle of incidence. The displacement of a moving surface beneath the optical sensor (faced down) can be determined by analyzing the changes between two consecutive images $(I_{i-1}$ and $I_i)$ as illustrated in Figure 3(b), where the black pixels represent the common area in both images; while hashed pixels are the intensity changes as detected by the sensor. The instantaneous velocity of the moving surface at a particular time instant can be expressed as

$$\mathbf{v} = v_x \hat{x} + v_y \hat{y} \tag{1}$$

and

$$\begin{bmatrix} v_x \\ v_y \end{bmatrix} = \frac{1}{t_c} \begin{bmatrix} \Delta x \\ \Delta y \end{bmatrix} = \frac{1}{C_i t_c} \begin{bmatrix} C_x \\ C_y \end{bmatrix} \tag{2}$$

where $\hat{x}$ and $\hat{y}$ are unit vectors of the x and y axes defined in Figure 2; t_c is the cycle time; C_i is the sensor resolution in counts per unit length; and $(\Delta x, \Delta y)$ and (C_x, C_y) are the incremental distance traveled and the corresponding sensor outputs (in counts) within the cycle respectively.

For a 3D spherical wrist where the center of rotation is fixed, a pair of two-DOF sensors is adequate to measure the three-DOF rotational motions. Figure 3(c) shows the CAD models of a spherical optical encoder for measuring the three-

DOF orientation of a spherical body. The optical sensors that detect the surface motion of the rotor are fixed on the stator. The stator and the rotor are concentric and the gap between the stator and rotor surfaces is small as compared to the radius of the rotor. The objective of the spherical optical encoder is to determine the position and the spin of the rotor shaft.
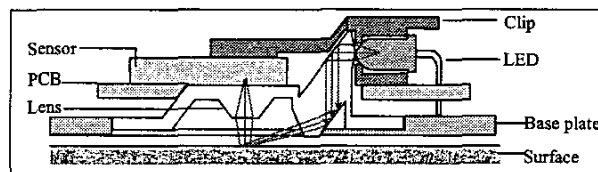
(a) Illustrative schematics
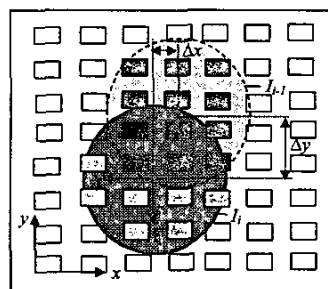
(b) Surface moved captured by two consecutive images
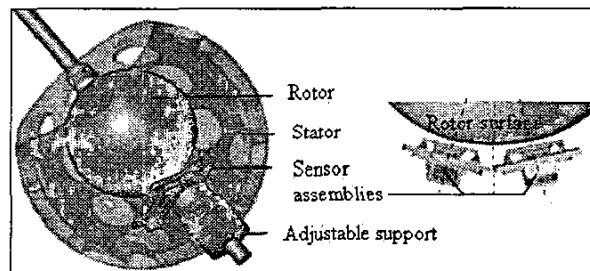
(c) Overview of a three-DOF spherical sensor

Figure 3 Structural overview of three-DOF spherical encoder

3. KINEMATICS OF A 3-DOF SPHERICAL ENCODER

Figure 4 defines the coordinate frames used in the following discussions, where the coordinate systems, *XYZ* and *xyz*, are the reference and the body-fixed coordinate frames attached at the centers of the stator and the rotor respectively. The z-axis intersects with the surface of the rotor at point P. The unit vector $\hat{z}$ (along the shaft or the z-axis in the rotor coordinate frame) can be expressed in the XYZ frame as

$$\hat{z} = \begin{bmatrix} \sin \gamma \cos \alpha & \sin \gamma \sin \alpha & \cos \gamma \end{bmatrix}^T \tag{3}$$

where γ is the angle between the Z and the z axes; and α is the angle between the projection of the z-axis on the *XY* plane and the *X* axis.

In order to have a means to verify the sensor kinematics experimentally, we develop a model based on an existing wrist

1597

apparatus (Figure 2, [Klement, 1997]). Mathematically, the rotor motion of the apparatus can be described by the angular velocity defined as follows:

$$\boldsymbol{\omega} = \omega_X \hat{X} + \omega_Y \hat{Y} + \omega_z \hat{z} \qquad (4)$$

where $\hat{X}$ and $\hat{Y}$ are unit vectors of the X and Y axes; and $\omega_X, \omega_Y, \omega_z$ are the angular velocities about the $\hat{X}, \hat{Y}$ and $\hat{z}$ respectively.

Without loss of generality, we consider that one of the two sensors is located along the Z axis on the spherical stator at O_1 as shown in Figure 4. The second sensor is placed on the same spherical surface at O_2 such that its optical axis is on the XZ plane. The optical axes of the two sensors meet at the spherical center but are spaced by an angle θ. Thus, the locations of O_1 and O_2 are given by

$$r_k = \begin{bmatrix} -R\sin\theta_k & 0 & R\cos\theta_k \end{bmatrix}^T \qquad (k=1,2) \qquad (5)$$

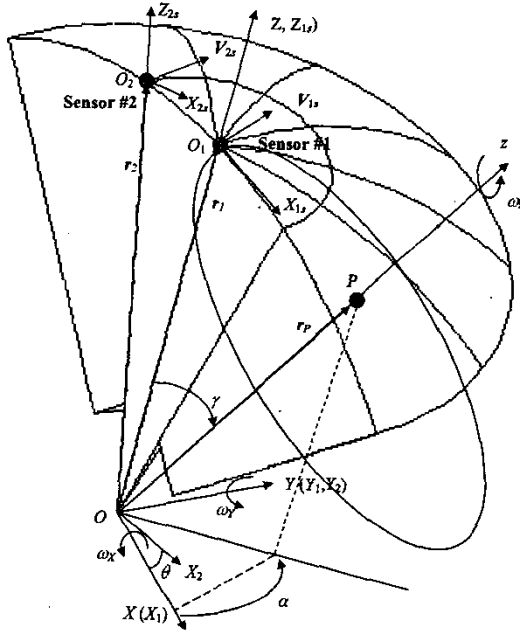where $\theta_1 = 0$; $\theta_2 = \theta$ and R is the radius of the rotor.

Figure 4 Coordinate systems

3.1 Forward Kinematics

The forward kinematics gives the instantaneous readouts of the sensors, Equation (2), in terms of the angular velocity in three orthogonal directions. Using Equation (3), the angular velocity of the rotor can be expressed in the stator reference frame:

$$\boldsymbol{\omega} = (\omega_X + \omega_z \sin\gamma\cos\alpha)\hat{X} + (\omega_Y + \omega_z \sin\gamma\sin\alpha)\hat{Y} + \omega_z \cos\gamma\hat{Z} \qquad (6)$$

Thus, the velocity of point O_k on the rotor surface in stator frame XYZ can be computed from

$$\mathbf{v}_k = \boldsymbol{\omega} \times \mathbf{r}_k \qquad (7)$$

where ω and r_k and are given by Equations (4) and (5) respectively. Similarly, the velocity of point O_k can be determined from the sensor, which can be expressed in XYZ frame as follows:

$$\begin{bmatrix} v_{xk} \\ v_{yk} \\ 0 \end{bmatrix} = T(\theta_k)\begin{bmatrix} v_{kX} \\ v_{kY} \\ v_{kZ} \end{bmatrix} \qquad (8)$$

where $T(\theta_k)$ is the coordinate transformation matrix (rotation about the Y-axis) between the stator and the sensor frames. Substituting $\mathbf{v}_k$ or (v_{kX}, v_{kY}, v_{kZ}) from Equation (7) into Equation (8) yields

$$\begin{bmatrix} v_{xk} \\ v_{yk} \end{bmatrix} = R\begin{bmatrix} 0 & 1 & \sin\gamma\sin\alpha \\ -\cos\theta_k & 0 & -\sin\gamma\sin\theta_k - \cos\theta_k \sin\gamma\cos\alpha \end{bmatrix}\begin{bmatrix} \omega_X \\ \omega_Y \\ \omega_z \end{bmatrix}$$

Consider the configuration of two sensors defined in Equation (5), and note that only three of the four equations are independent:

$$\begin{bmatrix} v_{x1} \\ v_{y1} \\ v_{y2} \end{bmatrix} = R\begin{bmatrix} 0 & 1 & \sin\gamma\sin\alpha \\ -1 & 0 & -\sin\gamma\cos\alpha \\ -c_\theta & 0 & -s_\theta\cos\gamma - c_\theta\sin\gamma\cos\alpha \end{bmatrix}\begin{bmatrix} \omega_X \\ \omega_Y \\ \omega_z \end{bmatrix} \qquad (9)$$

where $c_\theta = \cos\theta$ and $s_\theta = \sin\theta$.

3.2 Inverse Kinematics

The inverse kinematics recovers the orientation of the rotor (inclination and spin angle of the shaft) from the instantaneous readouts of the sensors, Equation (2). The following assumptions are made in order to derive a closed form solution implementation in real time:

(1) The cycle is short such that $\omega \approx \Delta\phi/\Delta t = \Delta\phi/t_c$.
(2) The initial values are known such that

$$\phi_{i+1} = \phi_i + \Delta\phi_i = \begin{bmatrix} \phi_{X,i} + \Delta\phi_{X,i} & \phi_{Y,i} + \Delta\phi_{Y,i} & \phi_{z,i} + \Delta\phi_{z,i} \end{bmatrix}^T$$

and the coordinate of point P, r_P or (x_p, y_p, z_p) is given by

$$x_P = z_P \tan(\phi_{Y,i} + \Delta\phi_{Y,i}) \qquad (10a)$$

$$y_P = z_P \tan(\phi_{X,i} + \Delta\phi_{X,i}) \qquad (10b)$$

$$x_P^2 + y_P^2 + z_P^2 = R^2 \qquad (10c)$$

(3) Changes are small within the cycle such that

$$\sin(\alpha + \Delta\alpha) \approx \sin\alpha + \Delta\alpha\cos\alpha \text{ and } \cos(\alpha + \Delta\alpha) \approx \cos\alpha + \Delta\alpha\sin\alpha.$$

On the basis of the above assumptions, the incremental rotational angles about X, Y and z axes during the ith cycle can be derived from Equation (9):

$$\begin{bmatrix} \Delta\phi_{X,i} \\ \Delta\phi_{Y,i} \\ \Delta\phi_{z,i} \end{bmatrix} = \frac{1}{Rs_\theta c_\gamma}\begin{bmatrix} 0 & s_\theta c_{\gamma i} + c_\theta s_{\gamma i} c_{\alpha i} & s_{\gamma i} c_{\alpha i} \\ s_\theta c_{\gamma i} & -c_\theta s_{\gamma i} s_{\alpha i} & s_{\gamma i} s_{\alpha i} \\ 0 & c_\theta & -1 \end{bmatrix}\begin{bmatrix} \Delta x_{1,i} \\ \Delta y_{1,i} \\ \Delta y_{2,i} \end{bmatrix} \qquad (11)$$

where $\gamma_i \neq \dfrac{\pi}{2}$ and $\theta \neq 0$;

1598

and $c_{\gamma i} = \cos\gamma_i$; $c_{\alpha i} = \cos\alpha_i$; $s_{\gamma i} = \sin\gamma_i$; and $s_{\alpha i} = \sin\alpha_i$.
Furthermore, since

$$\mathbf{r}_p = R\begin{pmatrix} \sin(\gamma_i + \Delta\gamma_i)\cos(\alpha_i + \Delta\alpha_i) \\ \sin(\gamma_i + \Delta\gamma_i)\sin(\alpha_i + \Delta\alpha_i) \\ \cos(\gamma_i + \Delta\gamma_i) \end{pmatrix} \qquad (12)$$

the shaft inclination at the $(i+1)^{\text{th}}$ cycle can be derived from Equations (10) and (12), which yield

$$\alpha_{i+1} \approx \alpha_i + \Delta\alpha_i = \text{atan2}\left(\frac{\tan(\phi_{X,i} + \Delta\phi_{X,i})}{\tan(\phi_{Y,i} + \Delta\phi_{Y,i})}\right) \qquad (13a)$$

$$\gamma_{i+1} \approx \gamma_i + \Delta\gamma_i =$$
$$\cos^{-1}\left(\frac{1}{\sqrt{1 + \tan^2(\phi_{Y,i} + \Delta\phi_{Y,i}) + \tan^2(\phi_{X,i} + \Delta\phi_{X,i})}}\right) \qquad (13b)$$

For completeness, the spin angle is

$$\varphi_{i+1} \approx \varphi_i + \Delta\phi_{z,i} \qquad (13c)$$

where $0 \le \gamma_{i+1} < \dfrac{\pi}{2}$ and $\pi \le \alpha_{i+1} < -\pi$.

3.3 Computational Singularities

For $\theta \ne 0$, there are two computational singularities in the inverse kinematics:

(1) When $|\phi_{Y,i} + \Delta\phi_{Y,i}| = 0$, Equation (13a) becomes singular, which corresponds to $\gamma_i = \alpha_i = 0$ (i.e. z and Z axes are coincident). It can be shown with Equation (9):

$$\Delta\phi_{X,i} = -\frac{\Delta y_1}{R}; \ \Delta\phi_{Y,i} = \frac{\Delta x_1}{R}; \text{ and } \Delta\phi_X = \frac{\Delta y_2 - \Delta y_1\cos\theta}{R\cos\theta}.$$

(2) Equation (11) becomes singular when $\gamma_i = \pi/2$, which corresponds to $\left|\phi_{Y,i} + \Delta\phi_{Y,i}\right| = \dfrac{\pi}{2}$ or $\left|\phi_{X,i} + \Delta\phi_{X,i}\right| = \dfrac{\pi}{2}$ in Equation (13b). Due to the page limit, we do not discuss further since it does not pose a problem for joints with a working range of $\gamma < \frac{\pi}{2}$.

4. EXPERIMENTAL RESULTS

A prototype has been developed to help demonstrate the concept feasibility and verify the algorithm for measuring the three-DOF orientation. The setup also provides a means to evaluate the sensor performance and identify key parameters that could significantly influence the sensor performance.

4.1 Prototype Spherical Sensor and Test-bed

Experiments for testing the spherical sensor are carried out on the mechanical wrist apparatus [Klement, 1997] as shown in Figures 2 and 5. The wrist has three stepper motors to provide 3-DOF rotations. These motors (referred here as X, Y and z motors) drive the spherical shell via a universal joint. With half-stepping and a 9:1 timing-belt pulley reduction, the X and Y motions have a resolution of 0.1° per step. The z-motor driven via a micro-stepping controller rotates at a resolution of 10,000 steps per inch (0.036°) with respect to the X and Y motors that

are fixed. Since it is desirable to keep all motors fixed, a universal joint is used to transmit the z-rotation regardless of the shaft position, which has a non-linear input-output relationship:

$$\theta_{out} = \tan^{-1}\left(\frac{\tan\theta_{in}}{\cos\gamma}\right) + \text{constant}$$

The shaft that rotates the shell covers a cone of 70° motors. To provide a random-featured surface, the shell is covered with a piece of fabrics.

Two HDNS-2000 optical sensors [Agilent Technologies, 2001] were employed for the prototype illustrated in Figure 3(c). To match the moving surface, the two sensors are housed in a holder fabricated using stereography as shown in Figure 6.
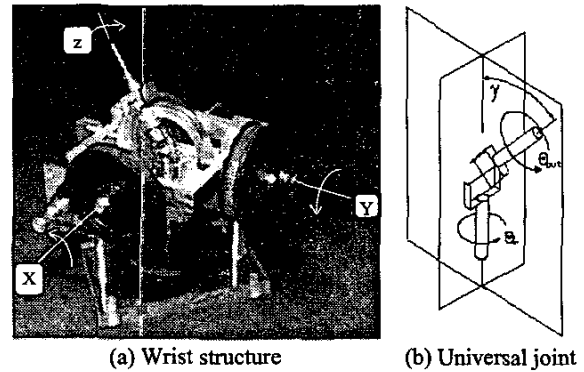

(a) Wrist structure   (b) Universal joint

Figure 5 Three-DOF wrist actuators

(a) Top   (b) Bottom

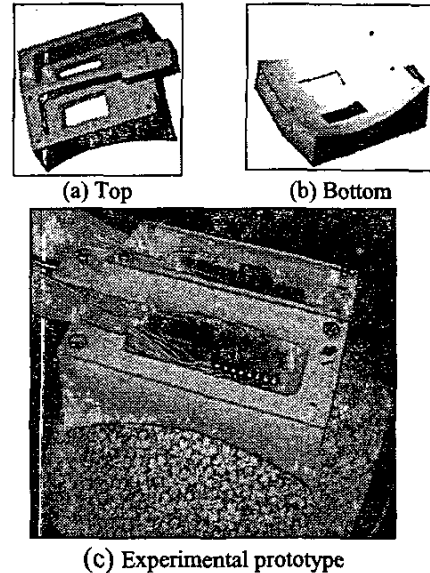

(c) Experimental prototype

Figure 6 CAD model and prototype mechanical holder

The following features were used to facilitate alignment of the sensors with the shell: (1) the two sensors face down with their optical axes pointing towards and intersecting at the center of the spherical shell. (2) The X_s axes of both sensors are

parallel to the X-axis of the reference frames such that both sensors have the same readouts in responding to rotations about the Y-axis only. (3) Since a single optical sensor is indifferent to rotations about its own optical axis, sensor #1 provides no information when the rotor shaft (or the z-axis) is in line with the Z-axis (of the stator reference frame).

The output signals of the optical sensors were decoded and computed in real time on a Pentium 650MHz PC with 512MB memory [Lee and Zhou, 2003]. Other values of the design parameters used in the experiments are summarized in Table 1.

4.2 Experimental Results

The rotor motion can be broadly categorized into two cases: (1) Rotations about the X axis, Y axis, or X and Y axes: These motions are translational as viewed by the optical sensor that detects local changes on a moving surface. Only one 2D sensor is sufficient for this measurement.

(2) Surface motion with rotations about the z-axis: In general, a pair of 2D sensors is needed for this motion.

Six different types of rotations (X, Y, XY, z, Xz, and XYz) were experimentally tested. Two motion commands are used; the first involves step changes of ϕ_X or ϕ_Y for α and γ going through 0 from 10° to -10°. The second is a monotonic decrement of ϕ_z. For each test, the initial location of the shaft is at $\alpha=\gamma=0$. The rotation angles (ϕ_X, ϕ_Y, ϕ_z) of the X, Y, z motors, along with the rotor shaft location (γ, α), are calculated and used as commands to drive the three steppers. Equations (11) and (13) are then used to recover the rotations (ϕ_X, ϕ_Y, ϕ_z) from the sensors.

The results comparing the specified values and the computed sensor data for the six types of rotations are summarized in Table 2. Graphical time-representations of the experimental results are shown in Figure 7, which correspond to the last case in Table 2. Figure 7(a) shows the four sensor readouts in counts. Figure 7(b) displays the computed rotations about X, Y and z axes. The shaft position (X_p, Y_p, Z_p) and inclination (γ, α) are given in Figures 7(c) and 7(d) respectively.

Table 1 Parameters of experimental prototype

| Design parameters	Values
Radius of spherical shell, R, mm (inch)	75 (3)
Sensor-surface spacing, mm	2
Sensor Resolution , counts per mm (counts per inch)	19.49 (495)
Sensor frame-rate, fps	1,500
Computer cycle time. ms	4.3538
Spacing between sensors, θ_y, degrees	22
Maximum γ in degrees	45

5. DISCUSSIONS OF RESULTS

As shown in Table 2, the maximum errors are less than 1° (in the order of the stepper resolution) for the four cases (X, Y, XY, z) that require only one sensor. The last two cases (X-z, Xyz) that require two sensors exhibit a larger error (but within
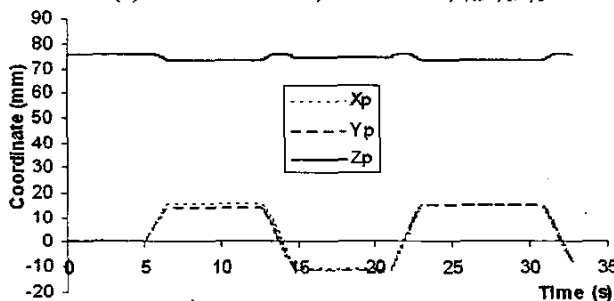
1.6°) as the two optical axes might have not met at the center of the moving surface as assumed.
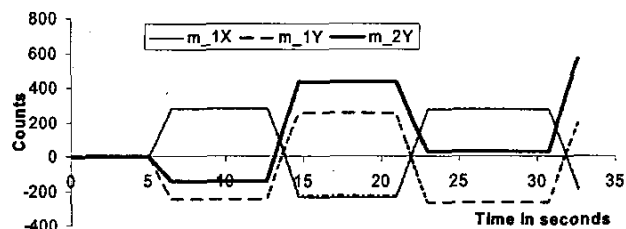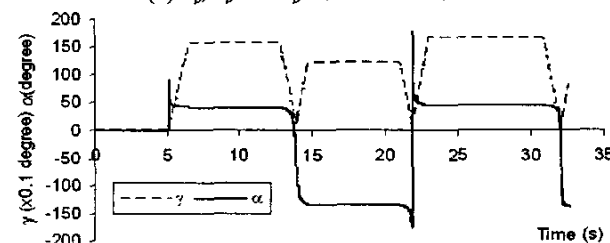

(a) Sensor counts
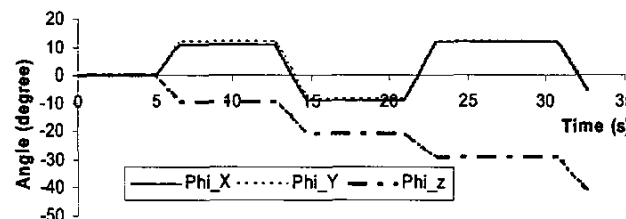
(b) Rotations about X, Y and z axes; ϕ_X, ϕ_Y, ϕ_z

(d) X_p, Y_p and Z_p as a function of time

(c) α and 10γ as a function of time

Figure 7 Experimental results

Figure 7(d) shows that the computed shaft inclination is sensitive around $\gamma=\alpha=0$. In order to study the effects of missed counts on the computation, simulations were carried out using the inverse kinematics, Equations (11)-(13). In each simulated calculations, white noises (-4, 0) in counts were superimposed to each of the four sensor readouts (all of which were assigned equal values; corresponding to a shaft inclination of 45°). The sensor data (with and without noises) were then used to compute the angles (ϕ_X, ϕ_Y, ϕ_z), the inclination (α, γ), and the shaft

1600

position $r_P(x_p, y_p, z_p)$. Figures 8(a)-(c) summarize the computed differences between with and without noises. As shown in Figure 8(a), missed counts have a larger influence in ϕ_z than in ϕ_X or ϕ_Y; in Figure 8(b), the computation of α is very sensitive in the neighborhood of $\gamma=0$ at which any missed count could cause $\alpha = \pi/4$ to $\alpha = \pi - (\pi/4) = 3\pi/4$ and vice versa, which well agrees with the experimental results in Figure 7(d). As shown in Figure 8(c), it is preferably to use the shaft position; the influence of missed counts has been kept within $200\mu m$ (or 4 times the resolution of the optical sensor, which is approximately $50\mu m$ per count).

Table 2 Summary of experimental results

Rotations	(ϕ_X, ϕ_Y, ϕ_Z) in degrees		
	Specified	Measured	Max. error
ϕ_X	(0, 0, 0)	(0.00, 0.00, 0.00)	
	(10, 0, 0)	(10.30, -0.09, 0.54)	0.54
	(-10, 0, 0)	(-10.26, -0.10, 0.04)	0.26
	(10, 0, 0)	(10.23, -0.19, 0.95)	0.95
	(-10, 0, 0)	(-10.30, 0.12, 0.10)	0.30
	(0, 0, 0)	(0.01, -0.10, 0.31)	0.31
ϕ_Y	(0, 0, 0)	(0, 0, 0)	
	(0, 10, 0)	(0.22, 10.04, -0.32)	0.32
	(0, -10, 0)	(0.02, -10.10, -0.17)	0.10
	(0, 10, 0)	(0.07, 10.20, 0.35)	0.35
	(0, -10, 0)	(0.32, -10.09, 0.32)	0.32
	(0, 0, 0)	(0.12, -0.14, 0.21)	0.21
ϕ_X, ϕ_Y	(0, 0, 0)	(0, 0, 0)	
	(10, 10, 0)	(10.10, 10.29, 0.20)	0.29
	(-10, -10, 0)	(-10.03, -10.04, -0.08)	0.08
	(10, 10, 0)	(10.03, 10.01, 0.13)	0.13
	(-10, -10, 0)	(-10.02, -10.01, 0.20)	0.20
ϕ_z	(0, 0, 0)	(0, 0, 0)	
	(0, 0, -10)	(0.01, 0.00, -10.07)	0.07
	(0, 0, -20)	(0.03, 0.00, -19.85)	0.15
	(0, 0, -30)	(0.10, 0.03, -29.83)	0.17
	(0, 0, -40)	(0.18, 0.10, -40.01)	0.18
	(0, 0, -50)	(0.30, 0.38, -50.00)	0.38
ϕ_X, ϕ_z	(0, 0, 0)	(0, 0, 0)	
	(0, 10, -10)	(0.15, 10.43, -9.86)	0.43
	(0, -10, -20)	(0.30, -10.34, -20.78)	0.78
	(0, 10, -30)	(0.51, 10.08, -30.00)	0.51
	(0, -10, -40)	(0.87, -10.21, -41.12)	1.12
ϕ_X, ϕ_Y, ϕ_z	(0, 0, 0)	(0, 0, 0)	
	(10, 10, -10)	(10.56, 11.60, -9.70)	1.60
	(-10, -10, -20)	(-8.97, -8.58, -21.09)	1.42
	(10, 10, -30)	(11.60, 11.60, -29.2)	1.60

REFERENCES

Agilent Technologies Inc., 2001, Solid-State Optical Mouse Sensor with PS/2 and Quadrature Outputs, Technical Data.

Bidlville, M., E. Raeber, J. Arreguit, H. Buczek, F. Van Shaik, F. Bauduin, and D. O'Keeffe, 1997, "Pointing Device Utilizing a Photo-detector Array," U.S. Patent No. 5,703,356, December 30.

Garner, H., M. Klement, and K-M. Lee, 2001, "Design and Analysis of an Absolute Non-Contact Orientation Sensor for Wrist Motion Control," AIM01 Proceedings, July 8–11, Como, Italy, pp. 69-74.

Klement, M. 1997 "Development of a Three DOF Vision-based Absolute Orientation Sensor," M. S. Thesis, ME, Georgia Tech.

Lee, K-M, 1995, Orientation Sensing System and Method for a Spherical Body, U.S. Patent 5,319,577, April 25.

Lee, K.-M. and R. Blenis, 1994, "Design Concept and Prototype Development of a Flexible Integrated Vision System," Journal of Robotic Systems, 11(5), 387-398.

Lee, K-M. and D. Zhou, 2003, "A Real-time Optical Sensor for Simultaneous Measurement of 3-DOF Motions," IEEE/ASME AIM03, Kobe Japan July 19-24.

Lee, K.-M., G. Meyouhas, and R. Blenis, 1993, "A Machine-Vision-Based Wrist Sensor for Direct Measurement of Three-DOF Orientation," Mechatronics, Vol. 3, No. 5, pp. 571-587.
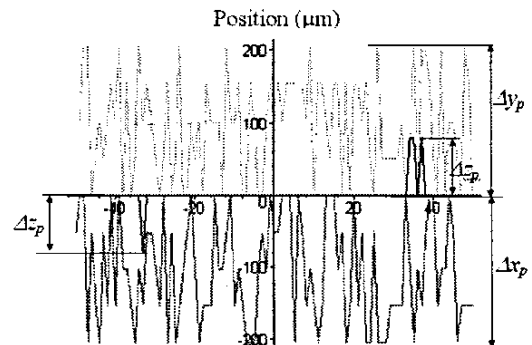
Lee, K.-M., R. Roth, and Z. Zhou, 1996 "Dynamic Modeling and Control of a Ball-joint-like Variable Reluctance Spherical Motor," ASME J. DSMC, Vol. 118, No. 1, pp.29-40.

(a) Errors in ϕ_X, ϕ_Y, ϕ_z

(b) Errors in α and γ
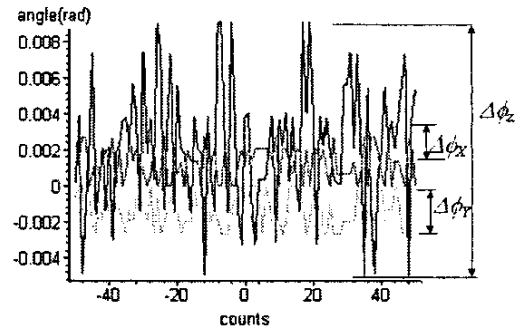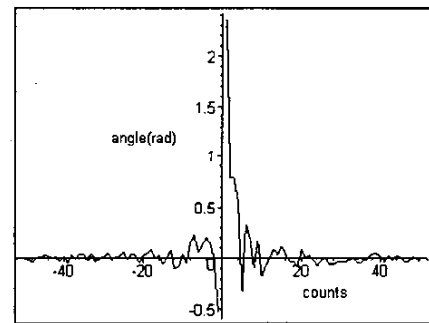
(c) Errors in x_p, y_p, z_p

Figure 8 Simulation results